Ballistic and Diffusive Thermal Conductivity of Graphene

Riichiro Saito,[1,*] Masashi Mizuno,[1] and Mildred S. Dresselhaus[2,3,†]
[1]Department of Physics, Tohoku University, Sendai 980-8578, Japan
[2]Department of Physics, Massachusetts Institute of Technology, Cambridge, Massachusetts 02139-4307, USA
[3]Department of Electrical Engineering, Massachusetts Institute of Technology, Cambridge, Massachusetts 02139-4307, USA

(Received 2 August 2017; revised manuscript received 22 September 2017; published 20 February 2018; corrected 27 February 2018)

This paper is a contribution to the Physical Review Applied *collection in memory of Mildred S. Dresselhaus.*

Phonon-related thermal conductivity of graphene is calculated as a function of the temperature and sample size of graphene in which the crossover of ballistic and diffusive thermal conductivity occurs at around 100 K. The diffusive thermal conductivity of graphene is evaluated by calculating the phonon mean free path for each phonon mode in which the anharmonicity of a phonon and the phonon scattering by a ^{13}C isotope are taken into account. We show that phonon-phonon scattering of out-of-plane acoustic phonon by the anharmonic potential is essential for the largest thermal conductivity. Using the calculated results, we can design the optimum sample size, which gives the largest thermal conductivity at a given temperature for applying thermal conducting devices.

DOI: 10.1103/PhysRevApplied.9.024017

I. INTRODUCTION

Thermal conductivity of suspended monolayer graphene has been reported to be very large up to 5300 W/mK at room temperature ($T = 300$ K) compared with copper (400 W/mK) or diamond (2000 W/mK) [1], which is important for possible application of heat-transfer materials or low-dimensional thermoelectric materials [2,3]. Thermal conductivity of graphene occurs mainly by phonons, while thermal conductivity of the conventional metal is mainly given by free electrons; this principle is known as the Wiedemann-Franz law [4]. The thermal conductivity of a phonon mode in the two-dimensional material is given by $Cv\ell/2$, where C, v, and ℓ denote, respectively, the heat capacity, the group velocity, and the mean free path of the phonon (MFP) [4]. The MFP ℓ is given by $\ell = v\tau$, where τ is the relaxation time of phonons that is determined by phonon-phonon scattering and phonon scattering by isotope.

Balandin and his co-workers have written comprehensive review articles on the thermal conductivity of 2D graphene, few-layer graphene, and one-dimensional (1D) graphene nanoribbon combined with their measurements, which contains comparison of theoretical methods and the difference of thermal conductivity between 2D or 1D graphene and 3D graphite [5–9]. Phonon thermal conductivity is large in graphene for the following reasons: (1) because of the high symmetry of graphene crystal, many anharmonic terms are suppressed or give relatively small values compared to low-symmetry materials; (2) the mass of a carbon atom is small, while large force constants of vibration exist due to the sp^2 covalent bonding; and (3) the in-plane acoustic phonon modes have large phonon mean free paths due to the lack of interlayer coupling of the phonons [5–9]. The small mass of a carbon atom with large force constants provides large group velocity for acoustic phonon modes with a large Debye temperature (2800 K) [10] of carbon compared to copper (343 K) [4].

Within the harmonic term of the crystal potential, the equation of motion for atoms can be diagonalized, from which we obtain phonon energy dispersion as a function of the phonon wave vector $\boldsymbol{q}$. When the anharmonic term of the crystal potential that is expressed by the cubic term of the vibrational amplitude is introduced to Hamiltonian, the phonon wave vectors are no longer good quantum numbers and phonon-phonon scattering occurs. By considering the anharmonic potential as a perturbation, the phonon relaxation time or MFP ℓ can be calculated as a function of $\boldsymbol{q}$ for each phonon mode, from which we can discuss the diffusive thermal conductivity. The diffusive thermal conductivity can be calculated by integrating the product $Cv\ell/2$ over the Brillouin zone in which (1) the heat capacity C of the material is calculated with the phonon density of states, (2) the group velocity v of the phonons is calculated with the phonon dispersion relation, and (3) the MFP is calculated with anharmonic terms. The total thermal conductivity is given as a function of T by

*rsaito@flex.phys.tohoku.ac.jp
†Deceased.

integrating $Cv\ell/2$ for all phonon modes and $\boldsymbol{q}$ over the Brillouin zone.

The MFP increases with decreasing T value, and diffusive thermal conductivity thus increases. When the MFP ℓ of the sth phonon mode is larger than the sample size L, ballistic thermal conductivity for the sth phonon mode occurs in which the phonon-distribution difference between the high-T side and the low-T side of the sample generates the heat flux, which is proportional to the product of the group velocity of the phonon and the heat capacity. The ballistic thermal conductivity monotonically decreases with decreasing T value since the heat capacity below the Debye temperature monotonically decreases to zero with decreasing T value to $T = 0$ K. Thus, the maximum thermal conductivity appears at a crossover temperature from diffusive to ballistic thermal conductivity, which should depend on the sample size L. In this paper, we calculate thermal conductivity of graphene as a function of T and L by the so-called force-constant model [11,12] while considering anharmonic force constants.

Chen and co-workers reported [13,14] that the thermal conductivity of a suspended single crystal of graphene monotonically increases with decreasing T value or with decreasing concentrations of an isotope of carbon, ^{13}C, up to 0%. The temperature dependence and the ^{13}C concentration dependence of the thermal conductivity above 300 K can be explained, respectively, by diffusive thermal conductivity and phonon scattering by ^{13}C because of the different mass of ^{12}C. If we estimate the MFP, we can predict that the thermal conductivity has a maximum at the lower temperature and then decreases with further decreasing T values because the heat capacity becomes zero at $T = 0$ K. Paulatto *et al.* calculated anharmonic properties of graphite and graphene by an *ab initio* calculation in which the phonon lifetime is expressed by the spectral width of phonon energy dispersions [15]. Anharmonic terms are obtained by empirical potentials, too, by other groups [16,17], though some empirical potentials do not reproduce the phonon energy dispersion and the potentials are not stable for a small displacement of atoms. Although the first-principles calculation does not require any empirical parameters, it is not clear from the calculated results which anharmonic terms are important for given T and L values. In this paper, using the symmetry analysis, we propose the dominant anharmonic terms of graphene whose values are fitted to reproduce the results of the experiment and the first-principles calculations. Our method can be used for other unknown materials once we can obtain anharmonic potential parameters by first-principles calculation [15,18].

Saito *et al.* calculated temperature dependence of ballistic thermal transport of electrons and phonons [19] in which they showed that some phonons contribute to the thermal conductivity diffusely, while other phonons contribute ballistically. Although we do not discuss how to control anharmonic terms for improving thermal conductivity, it is important when considering possible applications to understand the microscopic picture of the anharmonicity of graphene. In this paper, we focus only on the contribution from each phonon mode for a wide range of temperatures in which we predict a crossover from diffusive to ballistic thermal transport with decreasing temperature which depends on the sample size L.

The organization of this paper is as follows. In Sec. II, we show how to construct anharmonic terms of graphene with the tight-binding method. We will discuss the formulation of thermal conductivity for diffusive and ballistic thermal transport of phonons. In Sec. III, calculated results of thermal conductivity as a function of T and L will be shown for different concentrations of ^{13}C isotopes. In Sec. IV, a discussion and a summary are given.

II. METHOD

A. Anharmonic Hamiltonian

A Hamiltonian for the lattice vibration of graphene which includes third-order anharmonic terms is expressed by [20]

$$\begin{aligned}\mathcal{H} &= \mathcal{K} + \mathcal{V}_2 + \mathcal{V}_3 \\ &= \sum_i \frac{|\boldsymbol{p}_i|^2}{2m_i} + \frac{1}{2}\sum_{ij}\sum_{\alpha\beta}\Phi^{(ij)}_{\alpha\beta}u_{i\alpha}u_{j\beta} \\ &\quad + \frac{1}{3!}\sum_{ijk}\sum_{\alpha\beta\gamma}\Psi^{(ijk)}_{\alpha\beta\gamma}u_{i\alpha}u_{j\beta}u_{k\gamma}(\alpha,\beta,\gamma \in \{x,y,z\}), \quad (1)\end{aligned}$$

where $\mathcal{K}$, $\mathcal{V}_2$, and $\mathcal{V}_3$ denote, respectively, the kinetic energy, the harmonic potential, and the third-order anharmonic potential, and m_i, $\boldsymbol{p}_i$, and $\boldsymbol{u}_i$ denote, respectively, the mass, the momentum, and the displacement of the ith atom from its equilibrium position ($\boldsymbol{u} = 0$). $\Phi^{(ij)}$ and $\Psi^{(ijk)}$ are, respectively, the second- and third-rank tensors of forces that are defined by the second and third derivatives of potential V at the equilibrium position, which are given by [21]

$$\Phi^{(ij)}_{\alpha\beta} = \left.\frac{\partial^2 V}{\partial u_{i\alpha}\partial u_{j\beta}}\right|_0, \quad (2)$$

$$\Psi^{(ijk)}_{\alpha\beta\gamma} = \left.\frac{\partial^3 V}{\partial u_{i\alpha}\partial u_{j\beta}\partial u_{k\gamma}}\right|_0. \quad (3)$$

In a previous calculation of the phonon dispersion of graphene [11,12,22], we adopted the so-called force-constant model, in which the harmonic potential between the ith and jth atoms is given using a spring model such as

$$\mathcal{V}_2^{(ij)} = -\sum_{\alpha\beta}\frac{1}{2}\Phi^{(ij)}_{\alpha\beta}(u_{i\alpha} - u_{j\beta})^2. \quad (4)$$

When we consider the case of $i = j$ in the summation of i and j in Eq. (1), a quadratic term such as $\Phi_{\alpha\beta}^{(ij)} u_{i\alpha}^2$ in Eq. (4) is included in $\mathcal{V}_2$ in Eq. (1). Thus, we can adopt the force constant set in the previous calculation for obtaining the phonon dispersion. For given nearest-neighbor A and B_1 atoms that exist at $A(0,0,0)$ and B_1 $(a/\sqrt{3},0,0)$ (where $a = 2.46$ Å is the lattice constant of graphene [22]), respectively, we can select the following anharmonic terms,

$$\begin{aligned}\mathcal{V}_3^{(AB_1)} = &-\psi_r^{(1)}(u_{B_1x} - u_{Ax})^3 \\ &+ \psi_{ti}^{(1)}(u_{B_1x} - u_{Ax})(u_{B_1y} - u_{Ay})^2 \\ &+ \psi_{to}^{(1)}(u_{B_1x} - u_{Ax})(u_{B_1z} - u_{Az})^2, \end{aligned} \tag{5}$$

where $\psi_r^{(1)}$, $\psi_{ti}^{(1)}$, and $\psi_{to}^{(1)}$ denote, respectively, third order force-constant parameters for nearest-neighbor carbon atoms in radial (r), in-plane tangential (ti), and out-of-plane tangential (to) vibrations. In Fig. 1, we show corresponding third-order displacements for each term of Eq. (5). The first term of Eq. (5) represents the anharmonic term for the bond length. Since the increase of the potential energy is smaller for a case of expanding bond length $(u_{B_1x} - u_{Ax} > 0)$ than for a case of shrinking bond length $(u_{B_1x} - u_{Ax} < 0)$ in the hexagonal lattice, we can put the negative sign for $\psi_r^{(1)} > 0$ in Eq. (5). The second term of Eq. (5) represents the anharmonic effect of increasing energy with increasing interatomic distance by bending the bond $[(u_{B_1y} - u_{Ay})^2 > 0]$ in the direction of y (in plane) when the bond shrinks $(u_{B_1x} - u_{Ax} < 0)$. The third term of Eq. (5) represents the anharmonic effect of increasing energy by bending the bond $[(u_{B_1z} - u_{Az})^2 > 0]$ in the direction of z (out of plane) when the bond shrinks $(u_{B_1x} - u_{Ax} < 0)$.

Other anharmonic terms between the two atoms can be set to zero by considering the symmetry of the hexagonal lattice of graphene. For example, a third-order anharmonic term, $(u_{B_1y} - u_{Ay})^3$, is an odd function of $(u_{B_1y} - u_{Ay})$. However, since the potential V is invariant for the C_2 (or 180°) rotation around the center of the bond, the coefficient of the odd function should vanish. The same discussion can be taken for any pair of nth nearest-neighbor carbon atoms.

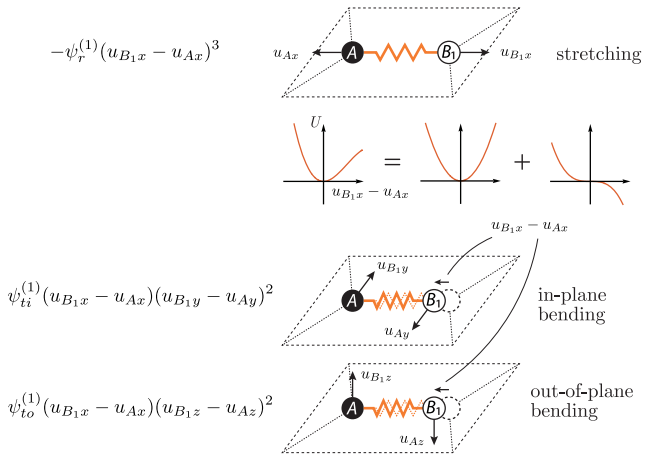

FIG. 1. Anharmonic terms for the pair of carbon atoms A and B_1 shown in Eq. (5).

For a given potential V, the potential and a third-order tensor such as $\Psi^{(AAB_1)}, \Psi^{(AB_1A)}, \Psi^{(AB_1B_1)}, \ldots, \Psi^{(B_1B_1A)}$ that is defined by Eq. (3) are related to one another by symmetry. For example, the nonzero terms of $\Psi^{(AAB_1)}$ are given by

$$\begin{aligned}\Psi_{xxx}^{(AAB_1)} &= -6\psi_r^{(1)}, \\ \Psi_{xyy}^{(AAB_1)} &= \Psi_{yxy}^{(AAB_1)} = \Psi_{yyx}^{(AAB_1)} = 2\psi_{ti}^{(1)}, \\ \Psi_{xzz}^{(AAB_1)} &= \Psi_{zxz}^{(AAB_1)} = \Psi_{zzx}^{(AAB_1)} = 2\psi_{to}^{(1)}. \end{aligned} \tag{6}$$

Since the potential V is an even function of z for monolayer graphene, all nonzero anharmonic terms have a factor of either u_z^2 or 1 (not u_z). Further, since the A and B_1 atoms exist along the x axis, a component such as xxy for the (AAB_1) pair should be zero. For a general pair of (ijk), we get the following 14 nonzero components by symmetry of $\Psi_{\alpha\beta\gamma}^{(ijk)}$: $\alpha\beta\gamma = xxx$, xxy, xyx, xyy, xzz, yxx, yxy, yyx, yyy, yzz, zzx, zzy, zxz, and zyz.

Once we obtain $\Psi^{(AAB_1)}$, the other term—$\Psi^{(AB_1A)}$, $\Psi^{(AB_1B_1)}$, etc.,—is given by the following relationship:

$$\Psi^{(iij)} = \Psi^{(iji)} = \Psi^{(jii)} = -\Psi^{(ijj)} = -\Psi^{(jij)} = -\Psi^{(jji)}. \tag{7}$$

Furthermore, for obtaining the tensor for the other pair of i, j, k atoms that does not exist along the x axis, we can use the rotation matrix U which connects to the i', j', k' atoms along the x axis to the i, j, k atoms,

$$\begin{aligned}&\sum_{\alpha\beta\gamma} \Psi_{\alpha\beta\gamma}^{(ijk)} u_{i\alpha} u_{j\beta} u_{k\gamma} \\ &\quad = \sum_{\alpha\beta\gamma} \Psi_{\alpha\beta\gamma}^{(i'j'k')} (U\boldsymbol{u}_i)_\alpha (U\boldsymbol{u}_j)_\beta (U\boldsymbol{u}_k)_\gamma \\ &\quad = \sum_{\substack{\alpha\beta\gamma \\ lmn}} \Psi_{\alpha\beta\gamma}^{(i'j'k')} U_{\alpha l} u_{il} U_{\beta m} u_{jm} U_{\gamma n} u_{kn} \\ &\quad = \sum_{lmn} \left(\sum_{\alpha\beta\gamma} \Psi_{\alpha\beta\gamma}^{(i'j'k')} U_{\alpha l} U_{\beta m} U_{\gamma n} \right) u_{il} u_{jm} u_{kn}. \end{aligned} \tag{8}$$

The phonon dispersion relation $\omega_s(\boldsymbol{k})$, $(s = 1, \ldots, 3N_{\text{atom}}$, where N_{atom} is the number of atoms in the unit cell) is calculated by solving the dynamical matrix [22] by taking the Fourier transform of u_j and by considering only the harmonic term $\mathcal{V}_2$. Then we can obtain the phonon eigenvectors, $\boldsymbol{e}(\kappa|\boldsymbol{q}s)$, $(\kappa = 1, \ldots, N_{\text{atom}})$ for the wave vector $\boldsymbol{q}$.

When we label u_j as $\boldsymbol{u}(\boldsymbol{l}\kappa)$ at the κth atom in the unit cell with lattice vector $\boldsymbol{l}$, the Fourier transform of $\boldsymbol{u}(\boldsymbol{l}\kappa)$ and its momentum $\boldsymbol{p}(\boldsymbol{l}\kappa)$ are given by

$$\boldsymbol{X}(\boldsymbol{q}\kappa) = \frac{1}{\sqrt{N}}\sum_{\boldsymbol{l}} \boldsymbol{u}(\boldsymbol{l}\kappa)\exp(-i\boldsymbol{q}\cdot\boldsymbol{l}), \tag{9}$$

$$\boldsymbol{P}(\boldsymbol{q}\kappa) = \frac{1}{\sqrt{N}}\sum_{\boldsymbol{l}} \boldsymbol{p}(\boldsymbol{l}\kappa)\exp(i\boldsymbol{q}\cdot\boldsymbol{l}), \tag{10}$$

where N denotes the number of unit cells in the crystal. Furthermore, $\boldsymbol{X}(\boldsymbol{q}\kappa)$ and $\boldsymbol{P}(\boldsymbol{q}\kappa)$ can be expressed by a linear combination of the phonon eigenvectors $\boldsymbol{e}(\kappa|\boldsymbol{q}s)$,

$$\boldsymbol{X}(\boldsymbol{q}\kappa) = \sum_{s} X_{\boldsymbol{q}s}\boldsymbol{e}(\kappa|\boldsymbol{q}s), \tag{11}$$

$$\boldsymbol{P}(\boldsymbol{q}\kappa) = \sum_{s} P_{\boldsymbol{q}s}\boldsymbol{e}^{*}(\kappa|\boldsymbol{q}s), \tag{12}$$

where $X_{\boldsymbol{q}s}$ and $P_{\boldsymbol{q}s}$ are, respectively, operators of the amplitude and the momentum for the sth phonon energy band. Defining the annihilation and creation operators for the sth phonon mode as

$$X_{\boldsymbol{q}s} = -i\sqrt{\frac{\hbar}{2m_\kappa\omega_{\boldsymbol{q}s}}}(a^{\dagger}_{\boldsymbol{q}s} - a_{-\boldsymbol{q}s}), \tag{13}$$

$$P_{\boldsymbol{q}s} = \sqrt{\frac{\hbar m_\kappa\omega_{\boldsymbol{q}s}}{2}}(a_{\boldsymbol{q}s} + a^{\dagger}_{-\boldsymbol{q}s}), \tag{14}$$

the Hamiltonian for the harmonic oscillation, $\mathcal{H}_0 = \mathcal{K} + \mathcal{V}_2$, and the anharmonic Hamiltonian $\mathcal{V}_3$ are, respectively, written as

$$\mathcal{H}_0 = \mathcal{K} + \mathcal{V}_2 = \sum_{\boldsymbol{q}s}\hbar\omega_{\boldsymbol{q}s}\left(a^{\dagger}_{\boldsymbol{q}s}a_{\boldsymbol{q}s} + \frac{1}{2}\right) \tag{15}$$

and

$$\mathcal{V}_3 = \frac{1}{3!}\sum_{\boldsymbol{q}s\boldsymbol{q}'s'\boldsymbol{q}''s''}\delta_{\boldsymbol{q}+\boldsymbol{q}'+\boldsymbol{q}'',\boldsymbol{G}}\Psi(\boldsymbol{q}s,\boldsymbol{q}'s',\boldsymbol{q}''s'') \times A_{\boldsymbol{q}s}A_{\boldsymbol{q}'s'}A_{\boldsymbol{q}''s''}, \tag{16}$$

where $A_{\boldsymbol{q}s}$ is defined by

$$A_{\boldsymbol{q}s} \equiv a^{\dagger}_{\boldsymbol{q}s} - a_{-\boldsymbol{q}s}. \tag{17}$$

$\Psi(\boldsymbol{q}s0\boldsymbol{q}'s',\boldsymbol{q}''s'')$ in Eq. (16) is the Fourier transform of $\Psi(\boldsymbol{0}\kappa,\boldsymbol{l}'\kappa',\boldsymbol{l}''\kappa'')$ that is written as

$$\begin{aligned}\Psi(\boldsymbol{q}s,\boldsymbol{q}'s',\boldsymbol{q}''s'') &= \frac{1}{\sqrt{N}}\sum_{\kappa,\kappa',\kappa''}\sqrt{\frac{\hbar^3}{8m_\kappa m_{\kappa'}m_{\kappa''}\omega_{\boldsymbol{q}s}\omega_{\boldsymbol{q}'s'}\omega_{\boldsymbol{q}''s''}}} \\ &\times\sum_{\boldsymbol{l}',\boldsymbol{l}''}\exp[i(\boldsymbol{q}'\cdot\boldsymbol{l}' + \boldsymbol{q}''\cdot\boldsymbol{l}'')]\sum_{\alpha\beta\gamma}\Psi_{\alpha\beta\gamma}(\boldsymbol{0}\kappa,\boldsymbol{l}'\kappa',\boldsymbol{l}''\kappa'') \\ &\times e_\alpha(\kappa|\boldsymbol{q}s)e_\beta(\kappa'|\boldsymbol{q}'s')e_\gamma(\kappa''|\boldsymbol{q}''s'').\end{aligned} \tag{18}$$

When we expand $A_{\boldsymbol{q}s}A_{\boldsymbol{q}'s'}A_{\boldsymbol{q}''s''}$ in Eq. (16) by using Eq. (17), we get the following processes: (1) three-phonon creation ($a^{\dagger}_{\boldsymbol{q}s}a^{\dagger}_{\boldsymbol{q}'s'}a^{\dagger}_{\boldsymbol{q}''s''}$), (2) one-phonon splits into two phonons ($a^{\dagger}_{\boldsymbol{q}s}a^{\dagger}_{\boldsymbol{q}'s'}a_{-\boldsymbol{q}''s''}$), (3) two phonons merging into one phonon ($a^{\dagger}_{\boldsymbol{q}s}a_{-\boldsymbol{q}'s'}a_{-\boldsymbol{q}''s''}$), and (4) three-phonon annihilation ($a_{-\boldsymbol{q}s}a_{-\boldsymbol{q}'s'}a_{-\boldsymbol{q}''s''}$). Since we discuss the phonon scattering process in thermal conductivity, we consider only processes (2) and (3), which satisfy energy conservation.

In Fig. 2, we show (a) the merging process and (b) the splitting process, where each process consists of the normal process ($\boldsymbol{G} = \boldsymbol{0}$) and the Umklapp process ($\boldsymbol{G} \neq \boldsymbol{0}$) in the momentum conservation, $\delta_{\boldsymbol{q}+\boldsymbol{q}'+\boldsymbol{q}'',\boldsymbol{G}}$, in Eq. (16).

In the case of the normal process, the total momentum of phonons or the heat flux does not change and thus does not contribute to the thermal resistivity, while, in the Umklapp process, since the total momentum can be changed by reciprocal lattice vectors, it can change the heat flux or thermal resistivity [4]. The normal process contributes to the relaxation of the distribution of phonons only at thermal equilibrium states.

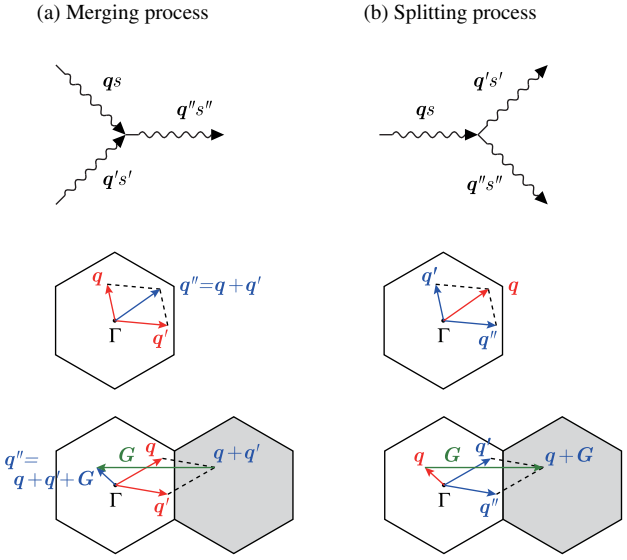

FIG. 2. (a) Merging process and (b) splitting process in the anharmonic Hamiltonian of Eq. (16) that contributes to the thermal conductivity. The momentum conservation, $\delta_{\boldsymbol{q}+\boldsymbol{q}'+\boldsymbol{q}'',\boldsymbol{G}}$, is shown for both the hexagonal Brillouin zone in which it is the normal process ($\boldsymbol{G} = \boldsymbol{0}$, middle panels) and in which it is the Umklapp process ($\boldsymbol{G} \neq \boldsymbol{0}$, bottom panels).

B. Diffusive thermal conductivity

There are two kinds of thermal conduction by phonons. One is diffusive conduction and the other is ballistic conduction. In diffusive conduction, the heat is transported by phonons that are scattered many times, while in the ballistic conductance, the heat is transported by phonons without scattering. If the sample size L is sufficiently larger than the MFP for each phonon mode, diffusive conduction occurs, while, when L is comparable to or smaller than the MFP, ballistic conductance occurs.

The definition of thermal conductivity κ is given by Fourier's law,

$$\boldsymbol{Q} = -\kappa \boldsymbol{\nabla} T, \tag{19}$$

in which $\boldsymbol{Q}$ and $\boldsymbol{\nabla} T$ represent, respectively, the heat flux per unit time and per unit cross section, and the temperature gradient. $\boldsymbol{Q}$ is given by

$$\boldsymbol{Q} = \frac{1}{V}\sum_{\boldsymbol{q}s} \hbar\omega_{\boldsymbol{q}s}(n_{\boldsymbol{q}s} - \bar{n}_{\boldsymbol{q}s})\boldsymbol{v}_{\boldsymbol{q}s}, \tag{20}$$

where $n_{\boldsymbol{q}s}$ and $\bar{n}_{\boldsymbol{q}s}$ denote, respectively, the number of phonons per unit volume for the wave vector $\boldsymbol{q}$ and for the sth phonon mode, as well as that for thermal equilibrium states. In Eq. (20), $\hbar\omega_{\boldsymbol{q}s}$ denotes the heat that the sth phonon carries, $n_{\boldsymbol{q}s} - \bar{n}_{\boldsymbol{q}s}$ represents an effective number of the phonons that contribute to the thermal conduction, $\boldsymbol{v}_{\boldsymbol{q}s}$ is the group velocity of the phonon, and V is the volume of the sample. As for the volume V, we adopt the conventional definition of volume for this problem as $V = N\Omega d_{\text{graphite}}$, where N, Ω, and $d_{\text{graphite}} = 3.35$ Å denote, respectively, the number of sampling points in the Brillouin zone, the area of the unit cell of graphene, and the interlayer distance between two graphene layers in graphite.

Here, we assume that the heat flux is parallel to the temperature gradient ($\boldsymbol{Q} \| \boldsymbol{\nabla} T$) and that the thermal conduction is isotropic in the two-dimensional plane. Then the diffusion thermal conductivity is given by

$$\begin{aligned}\kappa^{\text{diff}} &= -\frac{1}{2}\frac{\boldsymbol{Q}\cdot\boldsymbol{\nabla} T}{|\boldsymbol{\nabla} T|^2} \\ &= -\frac{1}{2V|\boldsymbol{\nabla} T|^2}\sum_{\boldsymbol{q}s}\hbar\omega_{\boldsymbol{q}s}(n_{\boldsymbol{q}s} - \bar{n}_{\boldsymbol{q}s})\boldsymbol{v}_{\boldsymbol{q}s}\cdot\boldsymbol{\nabla} T \\ &= \frac{\hbar^2}{2Vk_BT^2}\sum_{\boldsymbol{q}s}\omega_{\boldsymbol{q}s}^2\tau_{\boldsymbol{q}s}\bar{n}_{\boldsymbol{q}s}(\bar{n}_{\boldsymbol{q}s}+1)|v_{\boldsymbol{q}s}|^2. \end{aligned} \tag{21}$$

In the last line of Eq. (21), we use the following relationship from the Boltzmann equation:

$$n_{\boldsymbol{q}s} - \bar{n}_{\boldsymbol{q}s} = -\frac{\hbar\omega_{\boldsymbol{q}s}}{k_BT^2}\bar{n}_{\boldsymbol{q}s}(\bar{n}_{\boldsymbol{q}s}+1)\tau_{\boldsymbol{q}s}\boldsymbol{v}_{\boldsymbol{q}s}\cdot\boldsymbol{\nabla} T. \tag{22}$$

The derivation of Eq. (22) is given in Appendix A.

We can define the specific heat of lattice $C_{v\boldsymbol{q}s}$, per unit volume, for the sth phonon mode at $\boldsymbol{q}$ and the specific heat of lattice C_v, per unit weight, as, respectively,

$$\begin{aligned} C_{v\boldsymbol{q}s} &= \frac{\hbar^2}{Vk_BT^2}\omega_{\boldsymbol{q}s}^2\bar{n}_{\boldsymbol{q}s}(\bar{n}_{\boldsymbol{q}s}+1), \\ C_v &= \frac{V}{2Nm_C}\sum_{\boldsymbol{q}s}C_{v\boldsymbol{q}s}. \end{aligned} \tag{23}$$

Using Eq. (23), the diffusive thermal conductivity [Eq. (21)] is conventionally expressed by the product of $C_{v\boldsymbol{q}s}$, the MFP $\boldsymbol{\Lambda}_{\boldsymbol{q}s} = \tau_{\boldsymbol{q}s}\boldsymbol{v}_{\boldsymbol{q}s}(\|\boldsymbol{v}_{\boldsymbol{q}s})$, and the group velocity $\boldsymbol{v}_{\boldsymbol{q}s}$ as follows [2]:

$$\kappa^{\text{diff}} = \frac{1}{2}\sum_{\boldsymbol{q}s}C_{v\boldsymbol{q}s}\boldsymbol{\Lambda}_{\boldsymbol{q}s}\cdot\boldsymbol{v}_{\boldsymbol{q}s}. \tag{24}$$

C. Ballistic thermal conductivity

If L is smaller than the MFP, the phonon can propagate from one end to the other without scattering. In this case, we can assume that the phonon moves in one direction from the high-temperature side to the low-temperature side with the group velocity [19]. Making a comparison with Eq. (24), the ballistic thermal conductivity is given by [18]

$$\kappa^{\text{ball}} = L\sum_{\boldsymbol{q}s}C_{v\boldsymbol{q}s}v_{\boldsymbol{q}sx}\Theta(v_{\boldsymbol{q}sx}), \tag{25}$$

where $\Theta(v_{\boldsymbol{q}sx})$ is either 1 for $v_{\boldsymbol{q}sx} > 0$ (a right-going phonon) or 0 for $v_{\boldsymbol{q}sx} < 0$ (a left-going phonon). If we take the ratio $\kappa_{\boldsymbol{q}s}^{\text{diff}}/\kappa_{\boldsymbol{q}s}^{\text{ball}}$, we get

$$\frac{\kappa_{\boldsymbol{q}s}^{\text{diff}}}{\kappa_{\boldsymbol{q}s}^{\text{ball}}} = \frac{\pi|\Lambda_{\boldsymbol{q}s}|}{2L}. \tag{26}$$

In order to discuss the crossover of the diffusive and ballistic conduction, we define the MFP for the sth phonon mode and for all phonons, respectively, given as a function of T, as follows:

$$\langle\Lambda_s\rangle = \frac{\sum_{\boldsymbol{q}}\kappa_{\boldsymbol{q}s}^{\text{diff}}}{\sum_{\boldsymbol{q}}\kappa_{\boldsymbol{q}s}^{\text{diff}}/|\Lambda_{\boldsymbol{q}s}|} = \frac{\sum_{\boldsymbol{q}}C_{v\boldsymbol{q}s}\boldsymbol{\Lambda}_{\boldsymbol{q}s}\cdot\boldsymbol{v}_{\boldsymbol{q}s}}{\sum_{\boldsymbol{q}}C_{v\boldsymbol{q}s}|v_{\boldsymbol{q}s}|}, \tag{27}$$

$$\langle\Lambda_{\text{All}}\rangle = \frac{\sum_{\boldsymbol{q}s}\kappa_{\boldsymbol{q}s}^{\text{diff}}}{\sum_{\boldsymbol{q}s}\kappa_{\boldsymbol{q}s}^{\text{diff}}/|\Lambda_{\boldsymbol{q}s}|} = \frac{\sum_{\boldsymbol{q}s}C_{v\boldsymbol{q}s}\boldsymbol{\Lambda}_{\boldsymbol{q}s}\cdot\boldsymbol{v}_{\boldsymbol{q}s}}{\sum_{\boldsymbol{q}s}C_{v\boldsymbol{q}s}|v_{\boldsymbol{q}s}|}. \tag{28}$$

Finally, using Eq. (26), we define the thermal conductivity κ that includes both κ^{diff} and κ^{ball} as follows:

$$\kappa = \sum_{\boldsymbol{q}s} \min\left\{\frac{\pi|\Lambda_{\boldsymbol{q}s}|}{2L}, 1\right\} \times \kappa^{\text{ball}}_{\boldsymbol{q}s} = \sum_{\boldsymbol{q}s} \begin{cases} \kappa^{\text{ball}}_{\boldsymbol{q}s} & \Lambda_{\boldsymbol{q}s} > 2L/\pi \\ \kappa^{\text{diff}}_{\boldsymbol{q}s} & \Lambda_{\boldsymbol{q}s} < 2L/\pi \end{cases}. \tag{29}$$

In this definition, for each $\boldsymbol{q}$ and sth phonon mode, if the MFP $\Lambda_{\boldsymbol{q}s}$ is smaller than $2L/\pi$, we adopt κ^{ball}, while, if the MFP is larger than $2L/\pi$, we adopt κ^{diff}.

D. Phonon scattering by isotope impurities

Finally, we briefly mention the phonon scattering by isotope impurities, which was discussed by Klemens [23]. Since the mass of atom $m_{l\kappa}$ depends on the position of atom $l\kappa$, the momentum of the atom at $l\kappa$ is written as

$$\boldsymbol{p}(l\kappa) = \sqrt{\frac{\hbar m_{l\kappa}}{2N}} \sum_{\boldsymbol{q}s} \sqrt{\omega_{\boldsymbol{q}s}}\, \boldsymbol{e}'^{*}(\kappa|\boldsymbol{q}s) \times (a_{\boldsymbol{q}s} + a^{\dagger}_{-\boldsymbol{q}s}) \exp(-i\boldsymbol{q}\cdot\boldsymbol{x}_{l\kappa}), \tag{30}$$

where $\boldsymbol{x}_{l\kappa}$ is an equilibrium position of an atom at $l\kappa$. When we define the averaged mass by

$$\bar{m} = \sum_i f_i m_i, \tag{31}$$

where f_i and m_i denote, respectively, the abundance and the mass of $i = {}^{12}\text{C}$ or ${}^{13}\text{C}$. The perturbation Hamiltonian for the mass difference between isotope atoms is written as [23]

$$H_{\text{md}} = \sum_{l\kappa} \frac{1}{2} \Delta m_{l\kappa} \frac{1}{\bar{m}^2} |\boldsymbol{p}(l\kappa)|^2 \quad (\Delta m_{l\kappa} = m_{l\kappa} - \bar{m}). \tag{32}$$

Using the following equation for $|\boldsymbol{p}(l\kappa)|^2$,

$$\begin{aligned} |\boldsymbol{p}(l\kappa)|^2 &= \boldsymbol{p}(l\kappa)\cdot\boldsymbol{p}^{\dagger}(l\kappa) \\ &= \frac{\hbar\bar{m}}{2N} \sum_{\boldsymbol{q}s,\boldsymbol{q}'s'} \sqrt{\omega_{\boldsymbol{q}s}\omega_{\boldsymbol{q}'s'}}\, \boldsymbol{e}'^{*}(\kappa|\boldsymbol{q}s)\cdot\boldsymbol{e}'(\kappa|\boldsymbol{q}'s') \\ &\quad \times (a_{\boldsymbol{q}s} + a^{\dagger}_{-\boldsymbol{q}s})(a^{\dagger}_{\boldsymbol{q}'s'} + a_{-\boldsymbol{q}'s'}) \exp[-i(\boldsymbol{q}-\boldsymbol{q}')\cdot\boldsymbol{x}_{l\kappa}], \end{aligned} \tag{33}$$

H_{md} of Eq. (32) is given as

$$H_{\text{md}} = \sum_{\boldsymbol{q}s,\boldsymbol{q}'s'} \frac{\hbar}{4N\bar{m}} \sqrt{\omega_{\boldsymbol{q}s}\omega_{\boldsymbol{q}'s'}} (a_{\boldsymbol{q}s}a^{\dagger}_{\boldsymbol{q}'s'} + a^{\dagger}_{-\boldsymbol{q}s}a_{-\boldsymbol{q}'s'}) \mathcal{M}^{\boldsymbol{q}'s'}_{\boldsymbol{q}s}, \tag{34}$$

where the matrix element $\mathcal{M}^{\boldsymbol{q}'s'}_{\boldsymbol{q}s}$ is expressed as

$$\mathcal{M}^{\boldsymbol{q}'s'}_{\boldsymbol{q}s} = \sum_{l\kappa} \Delta m_{l\kappa} \boldsymbol{e}'^{*}(\kappa|\boldsymbol{q}s)\cdot\boldsymbol{e}'(\kappa|\boldsymbol{q}'s') \exp[-i(\boldsymbol{q}-\boldsymbol{q}')\cdot\boldsymbol{x}_{l\kappa}]. \tag{35}$$

Using Fermi's "golden rule," the scattering probability from the $\boldsymbol{q}s$ phonon to the $\boldsymbol{q}'s'$ phonon is given by

$$\begin{aligned} P^{\boldsymbol{q}'s'}_{\boldsymbol{q}s} &= \frac{2\pi}{\hbar^2} |\langle n_{\boldsymbol{q}s}-1, n_{\boldsymbol{q}'s'}+1|H_{\text{md}}|n_{\boldsymbol{q}s}, n_{\boldsymbol{q}'s'}\rangle|^2 \delta(\omega_{\boldsymbol{q}'s'} - \omega_{\boldsymbol{q}s}) \\ &= \frac{\pi}{2(N\bar{m})^2} n_{\boldsymbol{q}s}(n_{\boldsymbol{q}'s'}+1)\omega_{\boldsymbol{q}s}\omega_{\boldsymbol{q}'s'} |\mathcal{M}^{\boldsymbol{q}'s'}_{\boldsymbol{q}s}|^2 \delta(\omega_{\boldsymbol{q}'s'} - \omega_{\boldsymbol{q}s}). \end{aligned} \tag{36}$$

The decreasing rate of the number of $\boldsymbol{q}s$ phonon is given by

$$-\left.\frac{\partial n_{\boldsymbol{q}s}}{\partial t}\right|_{\text{md}} = \sum_{\boldsymbol{q}'s'} (P^{\boldsymbol{q}'s'}_{\boldsymbol{q}s} - P^{\boldsymbol{q}s}_{\boldsymbol{q}'s'}), \tag{37}$$

and the spectral width of phonon energy dispersion due to the isotope impurity is expressed by

$$\tau^{-1}_{\boldsymbol{q}s(\text{md})} = \frac{\pi g}{2N} \sum_{\boldsymbol{q}'s'\neq\boldsymbol{q}s} \frac{\bar{n}_{\boldsymbol{q}'s'}+1}{\bar{n}_{\boldsymbol{q}s}+1} \omega_{\boldsymbol{q}s}\omega_{\boldsymbol{q}'s'} \mathcal{E}^{\boldsymbol{q}'s'}_{\boldsymbol{q}s} \delta(\omega_{\boldsymbol{q}'s'} - \omega_{\boldsymbol{q}s}), \tag{38}$$

where $\mathcal{E}^{\boldsymbol{q}'s'}_{\boldsymbol{q}s}$ represents the inner products of phonon eigenfunctions defined by

$$\mathcal{E}^{\boldsymbol{q}'s'}_{\boldsymbol{q}s} = \sum_{\kappa} |\boldsymbol{e}'^{*}(\kappa|\boldsymbol{q}s)\cdot\boldsymbol{e}'(\kappa|\boldsymbol{q}'s')|^2. \tag{39}$$

The derivation of Eq. (38) is shown in Appendix B. Since the formula for the spectra width contains the inner product of phonon eigenvectors $\mathcal{E}^{\boldsymbol{q}'s'}_{\boldsymbol{q}s}$ [Eq. (39)], the in-plane (or out-of-plane) phonon mode is scattered only to the same in-plane (or out-of-plane) phonon mode by the isotope impurities.

It is useful to define the averaged phonon frequency for a general isotope concentration. When we denote $\bar{m}_{\text{nat}}$ and ω_{nat} as the mass and the frequency for natural abundance of 1.1% ${}^{13}\text{C}$, the average phonon frequency is given by

$$\omega = \sqrt{\frac{\bar{m}_{\text{nat}}}{\bar{m}}}\omega_{\text{nat}}. \tag{40}$$

III. CALCULATED RESULTS

A. Phonon dispersion relations with spectral width

In order to calculate phonon dispersion relations, we adopt the harmonic force-constant parameters that we obtained in previous work [12] up to the 14th nearest neighbors by fitting the experimental results. As for anharmonic force

constants, we fit the force constants up to the fourth nearest neighbor (4NN) so as to reproduce the temperature dependence of experimental thermal conductivity for 1.1% natural abundance of ^{13}C [13,14]. We also try to fit the phonon dispersion relation with its spectral width by the first-principles calculation given by Paulatto *et al.* [15] for justifying that our fitting procedure to the experiment is reasonable.

In Table I, we show the anharmonic force constants up to 4NN in units of eV/Å^3 fitted to the experimental results (the top row) and the first-principles calculations (the bottom row). When we compare two of the anharmonic force-constant sets, we find that (1) the force constants for 1NN and 2NN give similar values to one another, but that (2) the force constants for 3NN and 4NN are rather different from one another. For example, we cannot adopt the 4NN value of ψ_{to}, $\psi_{to}^{(4)}$ since the $\psi_{to}^{(4)} > 0$ gives the opposite temperature dependence of thermal conductivity as that of the experimentally observed temperature dependence, and thus we cannot fit well to the experimental results. The difference between the fitted values for the 3NN and 4NN force constants and those by first-principles calculation is reasonable since we cut the range of anharmonic potential up to 4NN, while they consider a much longer range of anharmonic potential in the first-principles calculations. It is difficult for us to consider a long-distance anharmonic potential since we do not have sufficient information on experiments such as those involving a spectral width of phonon dispersion as a function of $\boldsymbol{q}$.

In Fig. 3, we plot phonon dispersion relations with their spectral width, which is magnified by 100 times. A large spectral width for a given s and $\boldsymbol{q}$ corresponds to large thermal resistivity. Furthermore, the phonon modes with lower energies contribute to thermal conductivity at lower values of T. Thus, as long as we consider $T < 700$ K, the spectral widths of the optical phonon modes such as longitudinal optical (LO), tangential optical (TO) and Z-axis optical (ZO, where Z indicates that the displacement vector is along Z axis) do not contribute to thermal resistivity since such phonons rarely exist. If we simply adopt the anharmonic potentials, we can see some singularly large spectra width at the Γ point or the crossing points of two phonon dispersion relations (not shown in Fig. 3). This singularity comes from the fact that the lowest-energy phonon mode near the Γ point, Z-axis accoustic (ZA, where Z indicates that the displacement vector is along the Z axis), can be easily excited by phonon-phonon scattering. In order to avoid such a singularity, we do not consider (for the sake of simplicity) the scattering process with ZA phonons for wave vectors smaller than $0.06|\Gamma\mathbf{K}|$. In fact, an out-of-plane phonon with such a long wavelength does not exist in the samples, in which we expect defects of the lattice and structural fluctuation, as the phonon is known to not be completely flat of graphene.

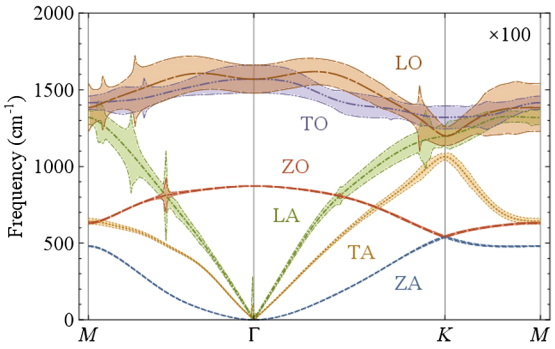

FIG. 3. Phonon dispersion with its spectral width by using anharmonic parameters fitted to the experimental results. The spectral width is magnified by 100 times.

TABLE I. Anharmonic force constant in units of eV/Å^3 by fitting to the experimental data (the top row) and by fitting to the first-principles calculation (the bottom row).

	ψ_r	ψ_{ti}	ψ_{to}
1NN	37.016	4.230	1.852
	37.275	5.270	4.379
2NN	−2.071	8.174	0.519
	−1.995	8.197	0.518
3NN	0.533	−0.433	−0.041
	0.331	−0.248	0.000
4NN	0.142	−1.262	⋯
	−0.244	−1.197	0.484

The phonons that contribute to thermal conduction are mainly ZA, transverse-acoustic (TA), and longitudinal-acoustic (LA) phonons that have relatively small energies. Even if we plot the spectral width of the phonon mode by considering only ψ_{to}, we can reproduce the spectral width of phonon modes below 900 cm^{-1}. Thus, we can say that the anharmonic force constant ψ_{to} is essential of total thermal resistivity. Furthermore, when we adopt the anharmonic force constants fitted to first-principles calculations, the calculated temperature dependence of thermal conductivity increases more slowly with decreasing values of T compared to that in the experiment. This is the reason we adopt to fit the anharmonic force constants to the experimental results.

In the calculation of thermal conductivity, the scattering of isotope impurity is also taken into account when we make a comparison to the experimental results. In Fig. 4, we plot the spectral width of the phonon dispersion relation for the case with 1.1% ^{13}C concentration, in which we consider not anharmonic terms but rather isotope effects for the spectral width, which is magnified by 1000 times. As is seen in Fig. 4, the spectral width is large for optical phonon modes. However, when we compare the spectral width in Fig. 4 to that in Fig. 3, the former is relatively small. Since the spectra width for isotope scattering is proportional to the phonon frequencies at initial and final phonon states

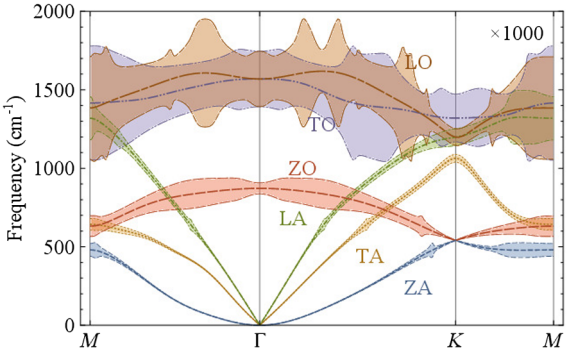

FIG. 4. The spectral width of phonon dispersion by scattering of a 1.1% ^{13}C isotope. The spectral width is magnified by 1000 times. In this plot, the spectra width of the phonon taken by anharmonicity is not taken into account.

[see Eq. (38)], the spectral width of ZA phonon is relatively small. It is noted that the spectral width of ZO phonon mode becomes small around the Γ point due to the fact that there are not many scattered phonon modes as the final state near the Γ point.

B. Thermal conductivity

In Fig. 5, we plot the calculated thermal conductivity as a function of temperature for ^{13}C concentrations of 0.0%, 1.1%, 50%, and 92.2%, using the fitting parameters that are fitted to the experimental results of 1.1% ^{13}C for the temperature region 300–750 K. Open and solid symbols denote, respectively, the calculated results and the experimental results of Chen *et al.* [13] for comparison. As seen in Fig. 5, the calculated thermal conductivity reproduces the experimental values for 300–750 K well—especially the fitted values for 1.1% and 99.2% ^{13}C, where the values are related to each other in a manner similar to isotope impurity, which is consistent with the experimental results. However, we can see a non-negligible deviation of the calculated results from the experiments for 50% and 0.0% ^{13}C for 300–500 K. In the case of 50% (or 0%) concentration, the scattering of phonons by a ^{13}C isotope cannot be expressed by perturbation [or by an approximation of relaxation time represented by a single phonon mode; see Eq. (B6)]. Thus, the quantitative analysis for a general concentration of ^{13}C has some limitations for temperatures lower than 500 K.

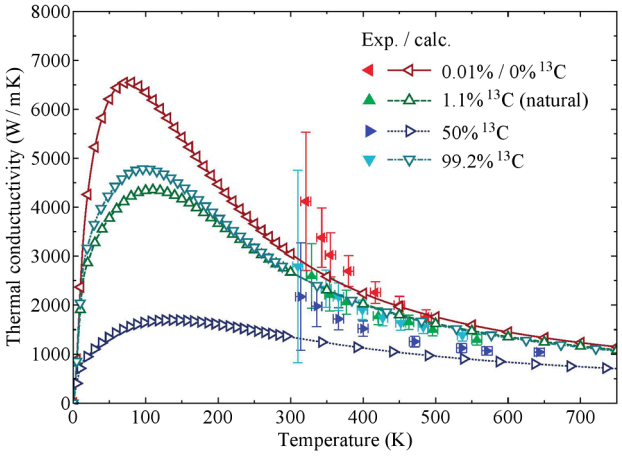

FIG. 5. Thermal conductivity as a function of temperature for several concentrations of ^{13}C using anharmonic force constants that are fitted to the experimental data for a natural abundance of 1.1% ^{13}C. For temperatures above 300 K, solid symbols denote the experimental data by Chen *et al.* [13], while, below 300 K, only theoretical calculated results are shown. Below 100 K, thermal conductivity decreases since the number of phonon decreases with decreasing temperature.

Although the experimental results are given only when $T > 300$ K, we extend the calculated results to the lower temperature region while using the same parameters. The calculated thermal conductivity shows a maximum at around 100 K for all cases of concentration of ^{13}C whose peak position appears at a lower temperature for a smaller concentration of ^{13}C. Increasing the thermal conductivity with decreasing values of T is explained by decreasing the phonon scattering events. If we further decrease T, thermal conductivity monotonically decreases to zero, which is explained by a decreasing number of phonons (or by a vanishing heat capacity), which is known to be a general behavior of thermal conductivity of a solid [24].

In Fig. 6, we show calculated thermal conductivity for 1.1% ^{13}C for different sample sizes L. The value of L can be considered the size of a single crystal of graphene in the polycrystalline sample. As shown in Fig. 6, the maxima of the thermal conductivity increases with increasing values of L at the lower temperature. It is for this reason that the criterion for selecting either ballistic or diffusive [Eq. (29)] depends on L. Once the MFP for any phonon mode is larger than L, the thermal conductivity becomes the ballistic thermal conductivity, κ^{ball}, which is proportional to L

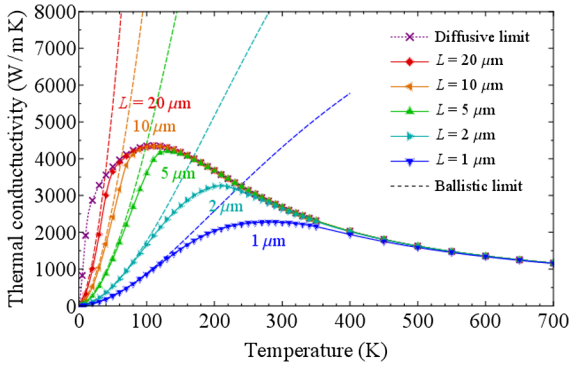

FIG. 6. Thermal conductivity for sample sizes $L = 1$, 2, 5, 10, and 20 μm. Here, we consider the isotope scattering by 1.1% ^{13}C. The dashed line for each L corresponds to the ballistic thermal conductivity, κ^{ball}, while the dotted lines represent diffusive thermal conductivity, κ^{diff}.

[see Eq. (25)] or the square of the number of phonons. In Fig. 6, we show the $\kappa^{\rm ball}$ by dashed line for each L as the ballistic limit. Furthermore, we also show $\kappa^{\rm diff}$ without considering the crossover to $\kappa^{\rm ball}$ shown by a dotted line as the diffusive limit. It is interesting to see that the thermal conductivity gives a different temperature dependence simply by changing L for the same sample quality of a crystal. The L-dependent thermal conductivity at low temperature is evidence of the crossover of thermal conductivity from diffusive to ballistic thermal conductivity which should be observed in the experiment. For a temperature larger than 300 K, on the other hand, since the MFP for each phonon mode is smaller than L, the L-dependent thermal conductivity does not appear anymore and the thermal conductivity is expressed only by diffusive thermal conductivity, in which phonon-phonon scattering is a dominant contribution to thermal resistivity.

IV. DISCUSSION AND SUMMARY

Finally, let us briefly comment on the application of graphene to thermal conductive devices. It is important to use the maximum thermal conductivity of graphene at relatively low temperature. However, as we can see in Fig. 6, if we use graphene at 300 K, the sample size $L = 2$ μm is already sufficient since thermal resistivity by phonon-phonon scattering is dominant. Even if we prepare a better quality of sample whose L value is larger than 2 μm, the value of thermal conductivity does not change at 300 K, which we can see in Fig. 6. On the other hand, when we increase L, we expect that the maximum value of thermal conductivity increases at lower temperatures. Nevertheless, $L = 10$ μm is already sufficiently large for the use of thermal conducting devices since the maximum of the diffusive limit has a maximum at around 100 K, as shown in Fig. 6. Such L-dependent thermal conductivity should be observed in the experiment even though there is some quantitative limitation of calculation. If we adopt a single crystal without any ^{13}C isotope, the maximum thermal conductivity becomes much larger (6500 W/mK in our calculation; not shown in this paper) than in the case of 1.1% ^{13}C, as shown Fig. 6 [18], and the maximum temperature for 0% ^{13}C decreases to 80 K. In this case, $L = 20$ μm is needed to obtain the maximum ballistic thermal conductivity at 80 K. Such behaviors should be checked experimentally in the future, too. It is important to note that the data in Fig. 6 do not mean that polycrystalline graphene is sufficient for temperatures higher than 400 K. It is for this reason that we do not consider the phonon scattering at the domain boundary of the polycrystalline sample, which might affect the thermal conductivity if the MFP is larger than L. When we consider the effect of phonon scattering at the boundary, we need to discuss the interference effect of multiple reflected phonons. It is important to note, in addition, that the ZA phonon modes that have the lowest phonon energy among the phonon modes are important for determining the average MFP or phonon occupation numbers. Thus, when we consider the ballistic and diffusive thermal conductivity, the ZA mode gives a dominant contribution to both effects of thermal conductivity. However, the ZA mode is sensitive to the substrate or stacking order of multilayer graphene, especially for the case of long wavelength. If we consider the ZA phonons near the Γ point, a large phonon scattering occurs for the crossing point of phonon dispersion, which would result in too much thermal resistivity to explain the experimental results. Thus, it is not clear from the present calculation what kind of substrate is the best for graphene thermal conducting devices. If we can control the ZA phonon modes and their anharmonicity, the thermal properties would be significantly improved, which is a problem to address in the future.

In conclusion, using a tight-binding description of harmonic and anharmonic vibration, we calculate the thermal conductivity in which not only phonon-phonon scattering, but also isotope scattering of phonons, is taken into account in the calculation. Fitting the harmonic and anharmonic force-constant sets to the experiment and the first-principles calculations, we calculate thermal conductivity as a function of temperature and the sample size L. In the low-temperature region, we see the maximum of thermal conductivity, and the thermal conductivity goes to zero with a further decreasing temperature. The maximum value of the thermal conductivity and the corresponding temperature depends on the sample size L for the same sample. It is for this reason that the crossover of diffusive thermal transport to ballistic thermal transport occurs with decreasing temperature.

ACKNOWLEDGMENTS

R. S. acknowledges MEXT KAKENHI Grants No. JP25107005 and No. JP15K21722. We sincerely thank the late Professor Mildred S. Dresselhaus for this collaboration; she passed away in February 2017 before finishing the project of thermal conductivity.

APPENDIX A: NUMBER OF PHONONS THAT CONTRIBUTE TO $\kappa_{\rm diff}$

Here, we derive Eq. (22). Occupation numbers of phonons, n_{qs}, as a function of time, are calculated using the Boltzmann equation,

$$\frac{\partial n_{qs}}{\partial t} = \left.\frac{\partial n_{qs}}{\partial t}\right|_{\rm diff} + \left.\frac{\partial n_{qs}}{\partial t}\right|_{\rm scatt} = 0, \tag{A1}$$

where the subscripts diff and scatt denote, respectively, diffusive and scattering terms. The diffusive terms can be given by

$$\left.\frac{\partial n_{\boldsymbol{q}s}}{\partial t}\right|_{\text{diff}} = -\boldsymbol{v}_{\boldsymbol{q}s}\cdot\boldsymbol{\nabla}T\frac{\partial n_{\boldsymbol{q}s}}{\partial T}, \tag{A2}$$

where $\boldsymbol{v}_{\boldsymbol{q}s} = \boldsymbol{\nabla}_{\boldsymbol{q}}\omega_{\boldsymbol{q}s}$ is the group velocity of the phonons at $\boldsymbol{q}s$ and $\boldsymbol{\nabla}T$ indicates the temperature gradient. $(\partial n_{\boldsymbol{q}s}/\partial T)\boldsymbol{\nabla}T$ represents the spacial change of the phonon occupation number caused by the temperature gradient. When we assume $n_{\boldsymbol{q}s} \simeq \bar{n}_{\boldsymbol{q}s}$ and thus $\partial n_{\boldsymbol{q}s}/\partial T \simeq \partial \bar{n}_{\boldsymbol{q}s}/\partial T$, Eq. (A2) can be written by defining $X_{\boldsymbol{q}s}$,

$$\left.\frac{\partial n_{\boldsymbol{q}s}}{\partial t}\right|_{\text{diff}} = -\boldsymbol{v}_{\boldsymbol{q}s}\cdot\boldsymbol{\nabla}T\frac{\partial \bar{n}_{\boldsymbol{q}s}}{\partial T} \equiv X_{\boldsymbol{q}s}. \tag{A3}$$

Here, we adopt the relaxation-time approximation (RTA) as follows:

$$-\frac{\partial n_{\boldsymbol{q}s}}{\partial t} = -\frac{\partial(n_{\boldsymbol{q}s}-\bar{n}_{\boldsymbol{q}s})}{\partial t} = \frac{n_{\boldsymbol{q}s}-\bar{n}_{\boldsymbol{q}s}}{\tau_{\boldsymbol{q}s}}, \tag{A4}$$

where $\tau_{\boldsymbol{q}s}$ is the relaxation time that determines how fast the $n_{\boldsymbol{q}s}$ decays. We define a dimensionless parameter $\psi_{\boldsymbol{q}s}$ in the Boltzmann distribution function for expanding $n_{\boldsymbol{q}s}$ [20],

$$\begin{aligned} n_{\boldsymbol{q}s} &= \left[\exp\left(\frac{\hbar\omega_{\boldsymbol{q}s}}{k_BT} - \psi_{\boldsymbol{q}s}\right) - 1\right]^{-1} \\ &\simeq n_{\boldsymbol{q}s}|_{\psi_{\boldsymbol{q}s}=0} + \left.\frac{\partial n_{\boldsymbol{q}s}}{\partial \psi_{\boldsymbol{q}s}}\right|_{\psi_{\boldsymbol{q}s}=0}\psi_{\boldsymbol{q}s} \\ &= \bar{n}_{\boldsymbol{q}s} + \bar{n}_{\boldsymbol{q}s}(\bar{n}_{\boldsymbol{q}s}+1)\psi_{\boldsymbol{q}s}. \end{aligned} \tag{A5}$$

Using Eq. (A5), Eq. (A4) can be written as [20]

$$-\frac{\partial n_{\boldsymbol{q}s}}{\partial t} = \frac{\bar{n}_{\boldsymbol{q}s}(\bar{n}_{\boldsymbol{q}s}+1)}{\tau_{\boldsymbol{q}s}}\psi_{\boldsymbol{q}s}. \tag{A6}$$

Furthermore, using the RTA in Eq. (A6) and defining $\Gamma_{\boldsymbol{q}s}$, the scattering term is given as follows:

$$\left.\frac{\partial n_{\boldsymbol{q}s}}{\partial t}\right|_{\text{scatt}} = -\frac{\bar{n}_{\boldsymbol{q}s}(\bar{n}_{\boldsymbol{q}s}+1)}{\tau_{\boldsymbol{q}s}}\psi_{\boldsymbol{q}s} \equiv -\Gamma_{\boldsymbol{q}s}\psi_{\boldsymbol{q}s}. \tag{A7}$$

Adding Eqs. (A3) and (A7) to the Boltzmann equation (A1), we get

$$X_{\boldsymbol{q}s} = \Gamma_{\boldsymbol{q}s}\psi_{\boldsymbol{q}s}. \tag{A8}$$

By solving the Boltzmann equation, we get $\psi_{\boldsymbol{q}s}$ as follows:

$$\begin{aligned} \psi_{\boldsymbol{q}s} &= \Gamma_{\boldsymbol{q}s}^{-1}X_{\boldsymbol{q}s} \\ &= \frac{\tau_{\boldsymbol{q}s}}{\bar{n}_{\boldsymbol{q}s}(\bar{n}_{\boldsymbol{q}s}+1)}X_{\boldsymbol{q}s} \\ &= -\frac{\hbar\omega_{\boldsymbol{q}s}}{k_BT^2}\tau_{\boldsymbol{q}s}\boldsymbol{v}_{\boldsymbol{q}s}\cdot\boldsymbol{\nabla}T. \end{aligned} \tag{A9}$$

Finally, using the definition of $\psi_{\boldsymbol{q}s}$ [Eq. (A5)], we get

$$\psi_{\boldsymbol{q}s} = \frac{n_{\boldsymbol{q}s}-\bar{n}_{\boldsymbol{q}s}}{\bar{n}_{\boldsymbol{q}s}(\bar{n}_{\boldsymbol{q}s}+1)}, \tag{A10}$$

and thus we get Eq. (22):

$$n_{\boldsymbol{q}s} - \bar{n}_{\boldsymbol{q}s} = -\frac{\hbar\omega_{\boldsymbol{q}s}}{k_BT^2}\bar{n}_{\boldsymbol{q}s}(\bar{n}_{\boldsymbol{q}s}+1)\tau_{\boldsymbol{q}s}\boldsymbol{v}_{\boldsymbol{q}s}\cdot\boldsymbol{\nabla}T. \tag{A11}$$

APPENDIX B: SPECTRAL WIDTH OF PHONON BY ISOTOPE SCATTERING

Here, we show that the spectral width by scattering of the phonons by isotope impurity is given by Eq. (38). Let us start the discussion by rewriting Eq. (36):

$$\begin{aligned} P_{\boldsymbol{q}s}^{\boldsymbol{q}'s'} &= \frac{2\pi}{\hbar^2}|\langle n_{\boldsymbol{q}s}-1, n_{\boldsymbol{q}'s'}+1|H_{\text{md}}|n_{\boldsymbol{q}s}, n_{\boldsymbol{q}'s'}\rangle|^2\delta(\omega_{\boldsymbol{q}'s'}-\omega_{\boldsymbol{q}s}) \\ &= \frac{\pi}{2(N\bar{m})^2}n_{\boldsymbol{q}s}(n_{\boldsymbol{q}'s'}+1)\omega_{\boldsymbol{q}s}\omega_{\boldsymbol{q}'s'}|\mathcal{M}_{\boldsymbol{q}s}^{\boldsymbol{q}'s'}|^2\delta(\omega_{\boldsymbol{q}'s'}-\omega_{\boldsymbol{q}s}). \end{aligned} \tag{B1}$$

If we assume that the isotope impurities distribute uniformly and randomly, we approximate $|\mathcal{M}_{\boldsymbol{q}s}^{\boldsymbol{q}'s'}|^2$ as follows,

$$\begin{aligned} |\mathcal{M}_{\boldsymbol{q}s}^{\boldsymbol{q}'s'}|^2 &= \mathcal{M}_{\boldsymbol{q}s}^{\boldsymbol{q}'s'}(\mathcal{M}_{\boldsymbol{q}s}^{\boldsymbol{q}'s'})^* \\ &= \sum_{l\kappa,l'\kappa'}\Delta m_{l\kappa}\Delta m_{l'\kappa'}\times[\boldsymbol{e}'^*(\kappa|\boldsymbol{q}s)\cdot\boldsymbol{e}'(\kappa|\boldsymbol{q}'s')][\boldsymbol{e}'^*(\kappa'|\boldsymbol{q}s)\cdot\boldsymbol{e}'(\kappa'|\boldsymbol{q}'s')]^*\times\exp[-i(\boldsymbol{q}-\boldsymbol{q}')\cdot(\boldsymbol{x}_{l\kappa}-\boldsymbol{x}_{l'\kappa'})] \\ &= \sum_{l\kappa}(\Delta m_{l\kappa})^2|\boldsymbol{e}'^*(\kappa|\boldsymbol{q}s)\cdot\boldsymbol{e}'(\kappa|\boldsymbol{q}'s')|^2 + \sum_{l'\kappa'\neq l\kappa}(\text{same as above}) \\ &\simeq N\sum_i f_i(\Delta m_i)^2\sum_\kappa|\boldsymbol{e}'^*(\kappa|\boldsymbol{q}s)\cdot\boldsymbol{e}'(\kappa|\boldsymbol{q}'s')|^2 \\ &= Ng\bar{m}^2\mathcal{E}_{\boldsymbol{q}s}^{\boldsymbol{q}'s'}, \end{aligned} \tag{B2}$$

where f_i and Δm_i denote, respectively, the concentration and the differing masses of isotopes $i = \{^{12}\mathrm{C}, ^{13}\mathrm{C}\}$. Here, we define g and $\mathcal{E}_{\boldsymbol{q}s}^{\boldsymbol{q}'s'}$ as follows:

$$g \equiv \sum_i f_i (1 - m_i/\bar{m})^2, \tag{B3}$$

and

$$\mathcal{E}_{\boldsymbol{q}s}^{\boldsymbol{q}'s'} \equiv \sum_\kappa |\boldsymbol{e}'^*(\kappa|\boldsymbol{q}s) \cdot \boldsymbol{e}'(\kappa|\boldsymbol{q}'s')|^2. \tag{B4}$$

Then Eq. (B1) is given by

$$P_{\boldsymbol{q}s}^{\boldsymbol{q}'s'} = \frac{\pi g}{2N} n_{\boldsymbol{q}s}(n_{\boldsymbol{q}'s'} + 1)\omega_{\boldsymbol{q}s}\omega_{\boldsymbol{q}'s'}\mathcal{E}_{\boldsymbol{q}s}^{\boldsymbol{q}'s'}\delta(\omega_{\boldsymbol{q}'s'} - \omega_{\boldsymbol{q}s}). \tag{B5}$$

The decreasing rate of phonons by isotope scattering per unit time is expressed by

$$\begin{aligned}
-\left.\frac{\partial n_{\boldsymbol{q}s}}{\partial t}\right|_{\mathrm{md}} &= \sum_{\boldsymbol{q}'s'} (P_{\boldsymbol{q}s}^{\boldsymbol{q}'s'} - P_{\boldsymbol{q}'s'}^{\boldsymbol{q}s}) \\
&= \sum_{\boldsymbol{q}'s'} \bar{P}_{\boldsymbol{q}s}^{\boldsymbol{q}'s'} (\psi_{\boldsymbol{q}s} - \psi_{\boldsymbol{q}'s'}) \\
&= \sum_{\boldsymbol{q}'s'} \frac{\pi g}{2N} \bar{n}_{\boldsymbol{q}s}(\bar{n}_{\boldsymbol{q}'s'} + 1)(\psi_{\boldsymbol{q}s} - \psi_{\boldsymbol{q}'s'})\omega_{\boldsymbol{q}s}\omega_{\boldsymbol{q}'s'} \\
&\quad \times \mathcal{E}_{\boldsymbol{q}s}^{\boldsymbol{q}'s'}\delta(\omega_{\boldsymbol{q}'s'} - \omega_{\boldsymbol{q}s}) \\
&= \sum_{\boldsymbol{q}'s' \neq \boldsymbol{q}s} \frac{\pi g}{2N} \bar{n}_{\boldsymbol{q}s}(\bar{n}_{\boldsymbol{q}'s'} + 1)\psi_{\boldsymbol{q}s}\omega_{\boldsymbol{q}s}\omega_{\boldsymbol{q}'s'} \\
&\quad \times \mathcal{E}_{\boldsymbol{q}s}^{\boldsymbol{q}'s'}\delta(\omega_{\boldsymbol{q}'s'} - \omega_{\boldsymbol{q}s}).
\end{aligned} \tag{B6}$$

In the last line, we use the so-called single-mode relaxation-time approximation. In this approximation, when we consider relaxation of a phonon mode, we postulate that the other phonon modes are in the thermal equilibrium states. This approximation makes the calculation simple since the relaxation of each phonon occurs independently. We believe that this approximation is justified as long as $n_{\boldsymbol{q}s}$ does not deviate much from $\bar{n}_{\boldsymbol{q}s}$. Finally, using the RTA [Eq. (A6)] for Eq. (B6), we get Eq. (38):

$$\tau_{\boldsymbol{q}s(\mathrm{md})}^{-1} = \frac{\pi g}{2N} \sum_{\boldsymbol{q}'s' \neq \boldsymbol{q}s} \frac{\bar{n}_{\boldsymbol{q}'s'} + 1}{\bar{n}_{\boldsymbol{q}s} + 1} \omega_{\boldsymbol{q}s}\omega_{\boldsymbol{q}'s'}\mathcal{E}_{\boldsymbol{q}s}^{\boldsymbol{q}'s'}\delta(\omega_{\boldsymbol{q}'s'} - \omega_{\boldsymbol{q}s}). \tag{B7}$$

[1] Alexander A. Balandin, Suchismita Ghosh, Wenzhong Bao, Irene Calizo, Desalegne Teweldebrhan, Feng Miao, and Chun Ning Lau, Superior thermal conductivity of single-layer graphene, Nano Lett. **8**, 902 (2008).

[2] L. D. Hicks and M. S. Dresselhaus, Thermoelectric figure of merit of a one-dimensional conductor, Phys. Rev. B **47**, 16631 (1993).

[3] L. D. Hicks and M. S. Dresselhaus, The effect of quantum well structures on the thermoelectric figure of merit, Phys. Rev. B **47**, 12727 (1993).

[4] C. Kittel, *Introduction to Solid State Physics*, 6th ed. (John Wiley & Sons, New York, 1986).

[5] A. A. Balandin, Thermal properties of graphene and nanostructured carbon materials, Nat. Mater. **10**, 569 (2011).

[6] D. L. Nika and A. A. Balandin, Two-dimensional phonon transport in graphene, J. Phys. Condens. Matter **24**, 233203 (2012).

[7] D. L. Nika, E. P. Pokatilov, and A. A. Balandin, Theoretical description of thermal transport in graphene: The issues of phonon cut-off frequencies and polarization branches, Phys. Status Solidi (b) **248**, 2609 (2011).

[8] S. Gosh, W. Bao, D. L. Nika, S. Subrina, E. P. Pokatilov, C. N. Lau, and A. A. Balandin, Dimensional crossover of thermal transport in few-layer graphene, Nat. Mater. **9**, 555 (2010).

[9] D. L. Nika and A. A. Balandin, Phonons and thermal transport in graphene and graphene-based materials, Rep. Prog. Phys. **80**, 036502 (2017).

[10] M. S. Fuhrer, Tuning the area of the fermi surface of graphene demonstrates the fundamental physics of electron-phonon scattering, Physics **3**, 106 (2010).

[11] R. Saito, T. Takeya, T. Kimura, G. Dresselhaus, and M. S. Dresselhaus, Raman intensity of single-wall carbon nanotubes, Phys. Rev. B **57**, 4145 (1998).

[12] R. Saito, M. Furukawa, G. Dresselhaus, and M. S. Dresselhaus, Raman spectra of graphene ribbons, J. Phys. Condens. Matter **22**, 334203 (2010).

[13] S. Chen, Q. Wu, C Mishra, J. Kang, H. Zhang, K. Cho, W. Cai, A. A. Balandin, and R. S. Ruoff, Thermal conductivity of isotopically modified graphene, Nat. Mater. **11**, 203 (2012).

[14] S. Chen, Q. Li, Q. Zhang, Y. Qu, H. Ji, R. S. Ruoff, and W. Cai, Thermal conductivity measurements of suspended graphene with and without wrinkles by micro-Raman mapping, Nanotechnology **23**, 365701 (2012).

[15] L. Paulatto, F. Mauri, and M. Lazzeri, Anharmonic properties from a generalized third-order *ab initio* approach: Theory and applications to graphite and graphene, Phys. Rev. B **87**, 214303 (2013).

[16] L. Lindsay and D. A. Broido, Optimized Tersoff and Brenner empirical potential parameters for lattice dynamics and phonon thermal transport in carbon nanotubes and graphene, Phys. Rev. B **81**, 205441 (2010).

[17] V. K. Tewary and B. Yang, Parametric interatomic potential for graphene, Phys. Rev. B **79**, 075442 (2009).

[18] M. Mizuno, master's thesis, Tohoku University, 2014 (in Japanese).

[19] K. Saito, J. Nakamura, and A. Natori, Ballistic thermal conductance of a graphene sheet, Phys. Rev. B **76**, 115409 (2007).

[20] G. P. Srivastava, *The Physics of Phonons* (CRC Press, London, 1990).

[21] A. A. Maradudin, E. W. Montroll, and G. H. Weiss, *Theory of Lattice Dynamics in the Harmonic Approximation* (Academic Press, New York, 1963).

[22] R. Saito, G. Dresselhaus, and M. S. Dresselhaus, *Physical Properties of Carbon Nanotubes* (Imperial College Press, London, 1998).

[23] P. G. Klemens, The scattering of low-frequency lattice waves by static imperfections, Proc. Phys. Soc. London Sect. A **68**, 1113 (1955).

[24] T. Takeuchi, N. Nagasako, R. Asahi, and U. Mizutani, Extremely small thermal conductivity of the Al-based Mackay-type 1/1-cubic approximants, Phys. Rev. B **74**, 054206 (2006).

Correction: The ordering of the second author's name was presented incorrectly and has been fixed.